Construction of Chirality-Sorting Optical Force Pairs

Man, Zhongsheng; Zhang, Yuquan; Cai, Yangjian; Yuan, Xiaocong; Urbach, H. P.

DOI
10.1103/PhysRevLett.133.233803

Publication date
2024

Document Version
Final published version

Published in
Physical review letters

Citation (APA)
Man, Z., Zhang, Y., Cai, Y., Yuan, X., & Urbach, H. P. (2024). Construction of Chirality-Sorting Optical Force Pairs. *Physical review letters*, *133*(23), Article 233803. https://doi.org/10.1103/PhysRevLett.133.233803

Construction of Chirality-Sorting Optical Force Pairs

Zhongsheng Man,[1,2,4] Yuquan Zhang,[5] Yangjian Cai,[3,4,*] Xiaocong Yuan,[5,6,†] and H. P. Urbach[2,‡]

[1]*School of Physics and Optoelectronic Engineering, Shandong University of Technology, Zibo 255000, China*
[2]*Optics Research Group, Delft University of Technology, Department of Imaging Physics, Lorentzweg 1, 2628CJ Delft, The Netherlands*
[3]*Shandong Provincial Engineering and Technical Center of Light Manipulation and Shandong Provincial Key Laboratory of Optics and Photonics Devices, School of Physics and Electronics, Shandong Normal University, Jinan 250014, China*
[4]*Collaborative Innovation Center of Light Manipulations and Applications, Shandong Normal University, Jinan 250358, China*
[5]*Nanophotonics Research Center, Shenzhen Key Laboratory of Micro-scale Optical Information Technology, Institute of Microscale Optoelectronics Shenzhen University, Shenzhen 518060, Guangdong, China*
[6]*Zhejiang Lab, Research Center for Humanoid Sensing, Research Institute of Intelligent Sensing, Hangzhou 311100, China*

(Received 24 May 2024; revised 28 October 2024; accepted 31 October 2024; published 4 December 2024)

Chiral objects are abundant in nature, and although the enantiomers have almost identical physical properties apart from their handedness, they can exhibit significantly different chemical properties and biological functions. This underscores the importance of sorting chiral substances. In this Letter, we demonstrate that chirality-sorting optical force pairs can be inversely generated in a tightly focused Gaussian beam by tailoring the input polarization state. We provide a detailed method for constructing the polarization state of the incident light to create the desired chiral optical field that generates the chirality-sorting optical force pairs. These force pairs precisely trap two opposite enantiomers at distinct predetermined positions within the same equilibrium plane, enabling their simultaneous identification and separation. Notably, the trapping positions and separation distances can be freely adjusted by altering the incident polarization parameters.

DOI: 10.1103/PhysRevLett.133.233803

Chirality refers to an asymmetry in which a structure cannot be superimposed onto its mirror image through any rotation or translation [1]. Enantiomers are the pairing of chiral compounds and their mirror images. Despite sharing many physical characteristics, enantiomers can have significantly different levels of toxicity and potency. In molecular biology, the chirality of an enantiomer is a key factor in determining whether its interaction with chiral resolving agents is favorable or not [2–5]. The identification and separation of enantiomers are, therefore, critical for both fundamental research and practical applications such as pharmaceuticals and agrochemicals.

Physically, when objects are immersed in optical fields, the interactions between light and matter can induce electric and magnetic polarizations that exert optical forces on the objects through the transfer of momenta and the presence of electromagnetic intensity gradients [6–21]. A range of optical manipulations using optical forces has been proposed and demonstrated, including trapping objects in potential minima [8,22,23] and pushing [6,24,25], pulling [26–31], rotating [32,33], or moving objects along complex trajectories and directions [34,35]. Indeed, when objects have chirality, additional different chiral polarizations may also emerge in light-matter interactions [36–39], leading to chirality-dependent optical forces that may be exploited for passive sorting of enantiomers. Crucially, optical methods provide nonimmersion and noncontact operations, distinguishing them from chemical methods and contributing to their growing popularity and attention [40–47]. Using the transverse spin angular momentum [48–51], significant advances have been achieved in generating chiral-separable lateral forces [52–54]. In addition, other optical chiral-selective sorting methods using polarization of light or specially designed platforms have also been proposed and demonstrated [55–67]. Most recently, gradient forces have been used in a subwavelength silicon-based waveguide platform to achieve nanometer-scale enantiomer separation. Strongly confined gradient fields are generated in the gap of the designed slot waveguides by counterpropagating pseudo-transverse-magnetic modes, resulting in stronger gradient forces compared to the relatively weak nonconservative lateral forces. Most importantly, the chiral gradient force causes the equilibrium position of the trapping force to deviate in the opposite direction from the center of the slit waveguide, depending on the handedness of the chiral particles [68]. Beyond their fundamental interest, these gradient forces could theoretically be useful for all-optical enantiomer sorting with an unstructured beam.

*Contact author: yangjiancai@sdnu.edu.cn
†Contact author: xcyuan@szu.edu.cn
‡Contact author: h.p.urbach@tudelft.nl

In this Letter, we demonstrate the generation of chirality-sorting optical force pairs that can accurately trap two opposite enantiomers at different predetermined positions within the same equilibrium plane. This enables the simultaneous identification and separation of enantiomers. To achieve this, we reverse the problem by structuring the transverse polarization configuration of an input field to create the desired chiral optical field, rather than designing the structures of an all-optical enantiomer sorting system. This approach generates the chirality-sorting optical force pairs and offers a simple and easy-to-implement solution. We then develop a rigorous analytical model to calculate the electromagnetic field and optical chirality density in the focal volume of the structured input field. Finally, we apply this method to demonstrate the simultaneous trapping of one enantiomer in one focus and the opposite enantiomer in the other focus within the same equilibrium plane, providing effective optical sorting of chiral particles.

For a spherical chiral particle with a radius a_p much smaller than the wavelength of light, the method of dipole approximation is precise enough to characterize the interaction between the chiral particle and the light fields. The time-averaged total optical forces exerted on a chiral dipole by a monochromatic electromagnetic wave are given by [27,52–54,67–70]

$$\begin{aligned}\langle \mathbf{F}\rangle = \nabla U + \frac{\sigma n}{c}\langle \mathbf{S}\rangle - \mathrm{Im}(\chi)\nabla\times\langle \mathbf{S}\rangle - \frac{c\sigma_e}{n}\nabla\times\langle \mathbf{L}_e\rangle \\ - \frac{c\sigma_m}{n}\nabla\times\langle \mathbf{L}_m\rangle + \omega\gamma_e\langle \mathbf{L}_e\rangle + \omega\gamma_m\langle \mathbf{L}_m\rangle \\ + \frac{ck^4}{12\pi n}\mathrm{Im}(\alpha_e\alpha_m^*)\mathrm{Im}(\mathbf{E}\times\mathbf{H}^*). \end{aligned} \tag{1}$$

Here, $U = [\mathrm{Re}(\alpha_e)|\mathbf{E}|^2/4] + [\mathrm{Re}(\alpha_m)|\mathbf{H}|^2/4] + \frac{1}{2}\mathrm{Re}(\chi)\mathrm{Im}(\mathbf{E}\cdot\mathbf{H}^*)$ is the optical potential, where α_e, α_m, and χ denote the electric, magnetic, and chiral polarizabilities of the particle, which are complex functions of the relative permittivity ε_p, relative permeability μ_p, and chirality parameter κ of the chiral particle [36,39,54,66,67]. $\mathbf{E}$ and $\mathbf{H}$ represent the electric and magnetic field vectors of the incident electromagnetic wave. Expressions $\langle \mathbf{S}\rangle = \mathrm{Re}(\mathbf{E}\times\mathbf{H}^*)/2$, $\langle \mathbf{L}_e\rangle = \varepsilon_0\varepsilon_1\mathrm{Im}(\mathbf{E}\times\mathbf{E}^*)/(4\omega)$, and $\langle \mathbf{L}_m\rangle = \mu_0\mu_1\mathrm{Im}(\mathbf{E}\times\mathbf{E}^*)/(4\omega)$ are the time-averaged Poynting vector and electric and magnetic spin angular momentum densities, whereas $\sigma_e = k\mathrm{Im}(\alpha_e)/(\varepsilon_0\varepsilon_1)$, $\sigma_m = k\mathrm{Im}(\alpha_m)/(\mu_0\mu_1)$, $\sigma=\sigma_e+\sigma_m-c^2k^4[\mathrm{Re}(\alpha_e\alpha_m^*+|\chi|^*)]/(6\pi n^2)$, $\gamma_e = 2\omega\mathrm{Im}(\chi) - ck^4\mathrm{Re}(\alpha_e\chi^*)/(3\pi\varepsilon_0\varepsilon_1 n)$, $\gamma_m = 2\omega\mathrm{Im}(\chi) - ck^4\mathrm{Re}(\alpha_m\chi^*)/(3\pi\mu_0\mu_1 n)$ represent light-beam cross sections, in which n denotes the refractive index of the medium surrounding the dipole; ε, μ, and k denote the relative permittivity, relative permeability, and wave number of the electromagnetic wave in the medium; and ε_0, μ_0, c, and ω the permittivity, permeability, speed, and frequency of light in the vacuum. Additional analyses are provided in Sec. S1 of the Supplemental Material [71].

Typically, gradient forces are more accessible and effective for trapping substances than nonconservative optical forces. Chiral substances possess one of two chiral states: left-handed or right-handed. If two distinct optical potentials can be generated within the same equilibrium plane—one trapping left-handed chiral particles and the other right-handed chiral particles—it becomes feasible to simultaneously identify and separate the two chiral substances using gradient forces. In the expression for the gradient forces in Eq. (1), the term $\mathrm{Im}(\mathbf{E}\cdot\mathbf{H}^*)/2$ is proportional to the optical chirality density [37–39] of the incident light. By creating a highly confined light field with a strong enough chiral distribution, where two opposite and spatially separated chiral densities exist, the desired light potential can be realized. Introducing a high numerical aperture (NA) objective lens enables the generation of strong gradient forces because of its tight focusing properties. The key lies in achieving the special chiral light field described above. The state of polarization (SoP), which is the vectorial property of the input light, plays a dominant role in a high NA objective focusing system [72,74,75]. In addition to being the simplest and most fundamental homogenous SoPs, light beams exhibit spatially inhomogeneous SoPs, known as vector optical fields. From theory, the SoP $|U\rangle$ for any given polarized light may be described as a two-dimensional Jones vector of two orthogonal polarization base vectors $|A\rangle$ and $|B\rangle$ [76,77],

$$|U\rangle = a_A|A\rangle + a_B|B\rangle, \tag{2}$$

where a_A and a_B are complex coefficients representing the contributions of the two bases. If the polarization vector is normalized, a_A and a_B can be expressed as $a_A = \cos\tau\exp(+i\psi)$ and $a_B = \sin\tau\exp(-i\psi)$, where $\tau\in[0,\pi/2]$ determines the fraction and ψ represents the additional relative phase between the two bases.

The electric and magnetic fields near the focus of an arbitrary polarized beam can be obtained using the Richards and Wolf vectorial diffraction theory [72],

$$\begin{bmatrix}\mathbf{E}\\ \mathbf{H}\end{bmatrix} = \frac{-ik}{2\pi}\iint_\Omega \begin{bmatrix}\mathbf{a}\\ \mathbf{b}\end{bmatrix}\cdot\exp[ik(\boldsymbol{s}\cdot\boldsymbol{r})]d\Omega, \tag{3}$$

where $k = 2\pi/\lambda$ denotes the wave number with λ the wavelength in image space, $\mathbf{a}$ and $\mathbf{b}$ denote the electric and magnetic strength vectors in the image space, s denotes the unit vector along a typical ray in image space, r the radius vector of arbitrary point $P(\rho_P, \varphi_P, z_P)$ in image space, and Ω the solid angle formed by all the geometrical rays that pass through the exit pupil of the system. In the original vector diffraction theory, the focus is located at the origin O(0,0,0) [72]; therefore, for an arbitrary point P near the focus in the image region, we have $\boldsymbol{s}\cdot\boldsymbol{r} = -\rho_P\sin\theta\cos(\phi-\varphi_P) + z_P\cos\theta$. In contrast, when the focus is shifted to another position $A(\delta x, \delta y, 0)$ in the transverse plane by radius vector $\boldsymbol{r}_{\mathrm{OA}} = (\delta x, \delta y, 0)$, the term $\boldsymbol{s} \cdot \boldsymbol{r}$ should be modified to $\boldsymbol{s} \cdot (\boldsymbol{r} - \boldsymbol{r}_{\mathrm{OA}}) = -\rho_P \sin\theta \cos(\phi - \varphi_P) + z_P \cos\theta + \delta x \sin\theta \cos\phi + \delta y \sin\theta \sin\phi$, which takes into account the spatial translation invariance of the focus. Physically, compared with situations in the absence of shifts, the input field is now modulated by an additional phase. When the high-NA objective lens obeys the sine condition, the corresponding phase distribution in the input pupil plane is given by

$$\vartheta = \frac{kr\mathrm{NA}}{r_0 n}(\delta x \cos\phi + \delta y \sin\phi), \tag{4}$$

where NA and n denote the numerical aperture of the objective lens and the refractive index in image space, r and r_0 the polar radius of the input optical field and pupil radial of the focusing system, and ϕ denotes the azimuthal angle in the objective space.

Theoretically, when ψ in Eq. (2) takes the form $\psi = \vartheta$, the resulting vector optical field exhibits simultaneous variation in both the radial and azimuthal directions, distinctly different from the well-known radially or azimuthally polarized beams. The two components of the $|A\rangle$ and $|B\rangle$ vibrations can be focused at different locations, $(\delta x, \delta y, 0)$ and $(-\delta x, -\delta y, 0)$. As a result, this allows the two vibration components to be spatially separated. Two SoPs at any pair of points on the standard Poincaré sphere with inverse symmetry with respect to the origin can serve as a pair of orthogonal polarization base vectors [73,76], $|A\rangle$ and $|B\rangle$ in Eq. (2) are chosen as $|A\rangle = (1/\sqrt{2})(\hat{e}_x - i\hat{e}_y)$ and $|B\rangle = (1/\sqrt{2})(\hat{e}_x + i\hat{e}_y)$ to obtain high enough optical chirality distributions near the focus (Sec. S2 [71]). They are, respectively, the right-handed and left-handed circularly polarized unit vectors. In addition, τ in Eq. (2) should be set to $\tau = \pi/4$ to achieve the equal magnitudes for the opposite chirality optical densities.

To verify theoretical predictions, we employ a Gaussian distribution input field with the polarization constructed above, the electromagnetic field in the image space of the strongly focused Gaussian input field in the pupil plane becomes

$$\begin{bmatrix}\mathbf{E}\\ \mathbf{H}\end{bmatrix} = -\frac{ikf}{2\pi}\int_0^{\alpha}\int_0^{2\pi}\sqrt{\cos\theta}\, e^{\{ik[-\rho_P \sin\theta\cos(\phi-\varphi_P)+z_P\cos\theta]\}} \times \exp\left(-\frac{\beta^2\sin^2\theta}{\sin^2\alpha}\right)\begin{bmatrix}\mathbf{V}_E\\ \mathbf{V}_H\end{bmatrix}\sin\theta\, d\phi\, d\theta, \tag{5}$$

where f denotes the focal distance, $\alpha = \arcsin(\mathrm{NA}/n)$ the maximum aperture angle, and β the ratio of the pupil radius to the beam waist, which we set to 1.5 in the calculations that follow. The vectors $\mathbf{V}_{\mathrm{E}}$ and $\mathbf{V}_{\mathrm{H}}$ represent the electric and magnetic field polarization vectors in the image space with their three components being (Sec. S3 [71])

$$\begin{aligned} V_{\mathrm{Ex}} &= \sin(\phi - C)\sin\phi + \cos(\phi - C)\cos\theta\cos\phi \\ V_{\mathrm{Ey}} &= -\sin(\phi - C)\cos\phi + \cos(\phi - C)\cos\theta\sin\phi \\ V_{\mathrm{Ez}} &= \cos(\phi - C)\sin\theta, \end{aligned} \tag{6}$$

$$\begin{aligned} V_{\mathrm{Hx}} &= D[-\cos(\phi - C)\sin\phi + \sin(\phi - C)\cos\theta\cos\phi] \\ V_{\mathrm{Hy}} &= D[\cos(\phi - C)\cos\phi + \sin(\phi - C)\cos\theta\sin\phi] \\ V_{\mathrm{Hz}} &= D[\sin(\phi - C)\sin\theta]. \end{aligned} \tag{7}$$

Here, $C = k\sin\theta(\delta x\cos\phi + \delta y\sin\phi)$ and $D = \sqrt{\varepsilon_0\varepsilon/\mu_0\mu}$.

Throughout this Letter, we set ψ in the input pupil according to Eq. (4) with $(\delta x, \delta y) = (1.5\lambda, 0)$, $(1.5\lambda, 1.5\lambda)$, and $(0, 1.5\lambda)$ (λ denoting the wavelength in the image space), the wavelength of incident light $\lambda_0 = 1.064$ um, input power 100 mW, $\mathrm{NA} = 1.2$, and $n = 1.33$. Given the above analysis, we expect to observe two foci in all three instances. For $(\delta x, \delta y) = (1.5\lambda, 0)$, the two foci lie along the x axis at $(1.5\lambda, 0, 0)$ and $(-1.5\lambda, 0, 0)$. For $(\delta x, \delta y) = (1.5\lambda, 1.5\lambda)$ and $(0, 1.5\lambda)$, the foci are located at $(1.5\lambda, 1.5\lambda, 0)$ and $(-1.5\lambda, -1.5\lambda, 0)$ as well as $(0, 1.5\lambda, 0)$ and $(0, -1.5\lambda, 0)$, respectively. The calculated total field intensity distributions in the focal plane (x-y plane at $z = 0$) are shown in Figs. 1(a)–1(c) for the above three instances. Clearly, twin foci with nearly identical profiles are obtained for all three instances. The positions of these foci are consistent with theoretical prediction. In addition, we anticipate opposite topological charges in the longitudinal component due to partial spin-to-orbital angular momentum conversion in this system [78,79]. The corresponding intensity [Figs. 1(d)–1(f)] and phase [Figs. 1(g)–1(i)] distributions of the longitudinal component are simulated for each instance. The electric field exhibits double doughnut-shaped intensity distributions, with anticlockwise and clockwise helical phase distributions. The results in Figs. 1(d)–1(i) are also in good agreement with theory. Once again, it demonstrates that in each of the three cases, one focus is contributed by the input component of the right-hand vibration, while the other focus is contributed by the input component of the left-hand vibration. Thus, we can expect to achieve a transformation in the light field that does not carry chirality into a chiral light field that carries local chirality densities of equal magnitude and opposite signs. From the optical chirality density distributions in the focal plane for the three input fields [Figs. 1(j)–1(l)], highly confined chiral optical fields are clearly generated, with spatially separated regions of opposite optical chirality density distributions that share the same profile but opposite signs in all three instances.

As examples, the optical force distributions of spherical chiral particles with radius $a_p = 40$ nm, relative permittivity $\varepsilon_p = 2.5$, permeability $\mu_p = 1$, and chirality parameter $\kappa = -1$ and 1 in the customized optical field of

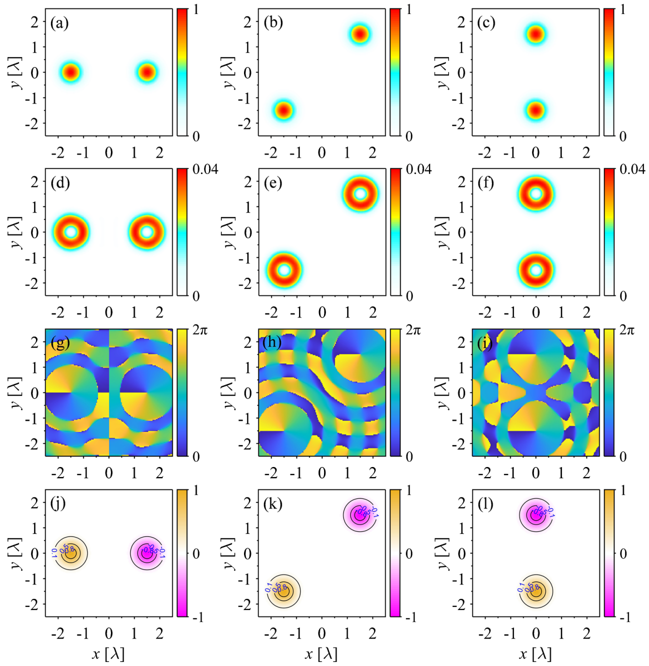

FIG. 1. Simulated electric field intensity and phase distributions, as well as the chirality density of tightly focused Gaussian beams in the x-y plane at $z = 0$ when $(\delta x, \delta y) = (1.5\lambda, 0)$ (left column), $(1.5\lambda, 1.5\lambda)$ (middle column), and $(0, 1.5\lambda)$ (right column); (a)–(c) intensity distributions for the total fields; (d)–(f) intensity distributions for the longitudinal component; (g)–(i) phase distributions for the longitudinal component; (j)–(l) optical chirality density distributions.

Fig. 1(a) are presented in Fig. 2. The effect of the chiral light field on different chiral substances is evident. For $\kappa = -1$, only the right focus allows a stable longitudinal trapping [Fig. 2(a)], whereas it is the left focus for $\kappa = 1$ [Fig. 2(b)]; nevertheless, both the equilibrium positions are approximately on the focal plane. In Fig. 2(c), the transverse optical force points toward the center of the right focus, resulting in a transverse trapping in the transverse plane. In contrast, the transverse force at any arbitrary position in the left focus directs away from the center, pushing the particle outward. The scenario is reversed when the handedness of the chiral particle is changed [Fig. 2(d)]. As a result, the identification and separation of chiral substances are achievable. Importantly, the position and distance between the separated enantiomer pairs can be precisely controlled using ψ according to Eq. (4) (Sec. S4 [71]).

To trace the physical sources of the optical forces acting on chiral particles, we set $\kappa = -1$ as a demonstration to study the contribution of each term of the optical force in Eq. (1) to the transverse force in the focal plane. Figures 3(a) and 3(b) show the transverse optical force distributions in the focal plane for the gradient force and the remaining optical forces, respectively. Although the non-gradient optical forces are nonzero, they are sufficiently

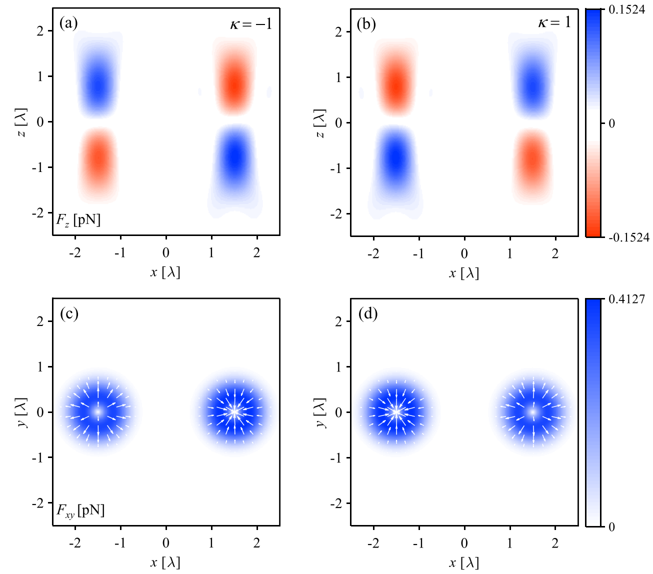

FIG. 2. Simulated distributions of (a),(b) longitudinal optical forces in the x-z plane at $y = 0$ and (c),(d) transverse optical forces in the x-y plane at $z = 0$ acting on the chiral particles with $a_p = 40$ nm and $\kappa = -1$ (left column) and 1 (right column) under a tightly focused Gaussian input field for $(\delta x, \delta y) = (1.5\lambda, 0)$ (white arrows indicate the direction of the optical forces).

weak that they can be neglected when compared with the gradient force in this setup. The gradient force arises from the direct chiral interaction between light and matter, the first two parts being the achiral optical forces related to the

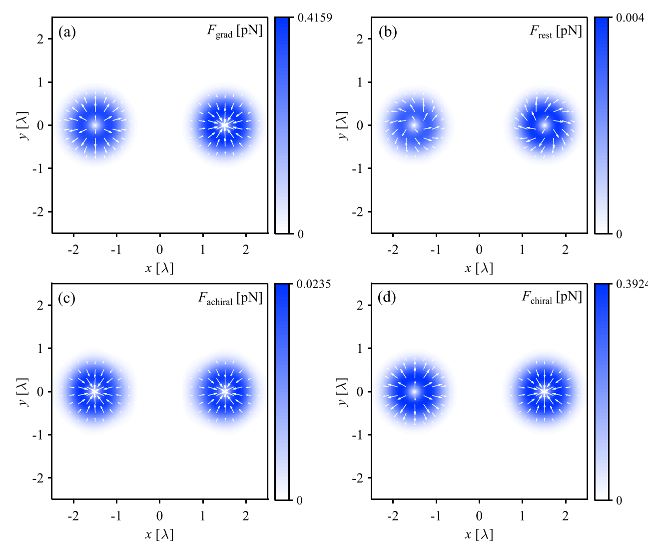

FIG. 3. Simulated transverse optical force distributions in the x-y plane at $z = 0$ for each term in Eq. (1), acting on chiral particles with $a_p = 40$ nm and $\kappa = -1$ under a tightly focused Gaussian input field for $(\delta x, \delta y) = (1.5\lambda, 0)$: (a) gradient force, (b) the remaining optical forces, (c) achiral optical forces, and (d) chiral optical forces (white arrows indicate the direction of the optical force).

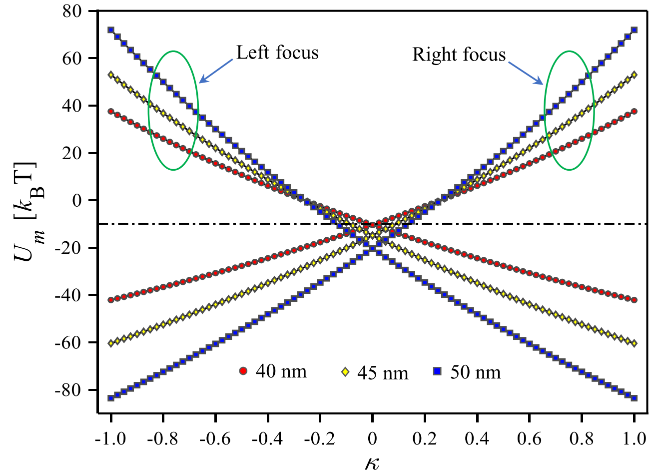

FIG. 4. Peak values of the trapping potential depth or barrier as a function of chirality parameter κ for the left and right foci in a tightly focused Gaussian input field for $(\delta x, \delta y) = (1.5\lambda, 0)$. The horizontal line represents the potential well of $-10\ k_B$T.

electric and magnetic energy densities and the third part being the chiral force associated with the optical chirality density. The transverse components of the achiral and chiral optical forces were specifically investigated [Figs. 3(c) and 3(d)]. Both the sign and magnitude of the achiral force remain the same in the twin foci. For the chiral force, however, the magnitude remains unchanged whereas the sign undergoes an inversion. In addition, the magnitude of the chiral force is significantly stronger than that of the achiral force, thereby enhancing the trapping at the right focus and weakening it at the left focus.

In the above analysis, the chirality values of the particle are -1 and 1. Figure 4 depicts the peak values of the trapping potential depth or barrier as a function of chirality parameter κ for the left and right foci in the constructed optical field. Particles of radii 45 and 50 nm were also included to study the influence of particle size on the trapping potential. Clearly, the curves for the left focus are opposite to those of the right focus, reaffirming that the twin foci exert opposite effects on the chiral particles. In addition, the trapping potential depth increases with increasing particle size and the absolute value of the chirality parameter. To achieve a stable trap, the trapping potential depth should be larger than 10 k_BT to overcome the kinetic energy of particles in Brownian motion [80]. Calculations show that, for particles of radii 40 nm, 45 nm, and 50 nm that can be trapped stably, the chirality parameter values should be larger than -0.0107, -0.0868, and -0.135 for the left focus and be less than 0.0107, 0.0868, and 0.135 for the right focus.

In conclusion, we have presented a straightforward method for generating chirality-sorting optical force pairs that can accurately trap two opposite enantiomers at distinct predesigned positions within the same equilibrium plane, thereby enabling effective optical sorting of chiral particles. We described how to choose the optical degrees of freedom of the transverse polarization structures for its realization. We developed a rigorous analytical model to calculate the electromagnetic field and optical chirality density in the focal volume of the proposed structured input field. The application of this method has the potential to expand the realm of customized structured light fields, paving the way for new advances in chiral particle sensing and imaging.

Acknowledgments—This work was partially supported by National Key Research and Development Program of China (2022YFA1404800, 2019YFA0705000); National Natural Science Foundation of China (12192254, 92250304, 12474294, 12074224, 61935013, 62375181, 61975133, W2441005); Natural Science Foundation of Shandong Province (ZR2021YQ02).

[1] W. T. B. Kelvin, *The Molecular Tactics of a Crystal* (Clarendon Press, Oxford, 1894).
[2] C. M. Dobson, Protein folding and misfolding, Nature (London) **426**, 884 (2003).
[3] H. Caner, E. Groner, L. Levy, and I. Agrant, Trends in the development of chiral drugs, Drug Discov. Today **9**, 105 (2004).
[4] C. Cecconi, E. A. Shank, C. Bustamante, and S. Marqusee, Direct observation of the three-state folding of a single protein molecule, Science **309**, 2057 (2005).
[5] B. S. Sekhon, Chiral pesticides, J. Pestic. Sci. **34**, 1 (2009).
[6] A. Ashkin, Acceleration and trapping of particles by radiation pressure, Phys. Rev. Lett. **24**, 156 (1970).
[7] A. Ashkin, Trapping of atom by resonance radiation pressure, Phys. Rev. Lett. **40**, 729 (1978).
[8] A. Ashkin, J. M. Dziedzic, J. E. Bjorkholm, and S. Chu, Observation of a single-beam gradient force optical trap for dielectric particles, Opt. Lett. **11**, 288 (1986).
[9] D. G. Grier, A revolution in optical manipulation, Nature (London) **424**, 810 (2003).
[10] Y. Roichman, B. Sun, Y. Roichman, J. Amato-Grill, and D. G. Grier, Optical forces arising from phase gradients, Phys. Rev. Lett. **100**, 013602 (2008).
[11] S. Albaladejo, M. I. Marqués, M. Laroche, and J. J. Sáenz, Scattering forces from the curl of the spin angular momentum of a light field, Phys. Rev. Lett. **102**, 113602 (2009).
[12] M. Padgett and R. Bowman, Tweezers with a twist, Nat. Photonics **5**, 343 (2011).
[13] K. Dholakia and T. Čižmár, Shaping the future of manipulation, Nat. Photonics **5**, 335 (2011).
[14] M. L. Juan, M. Righini, and R. Quidant, Plasmon nano-optical tweezers, Nat. Photonics **5**, 349 (2011).
[15] D. B. Ruffner and D. G. Grier, Optical forces and torques in nonuniform beams of light, Phys. Rev. Lett. **108**, 173602 (2012).
[16] R. W. Bowman and M. J. Padgett, Optical trapping and binding, Rep. Prog. Phys. **76**, 026401 (2013).
[17] O. M. Maragò, P. H. Jones, P. G. Gucciardi, G. Volpe, and A. C. Ferrari, Optical trapping and manipulation of nanostructures, Nat. Nanotechnol. **8**, 807 (2013).

[18] S. Sukhov and A. Dogariu, Non-conservative optical forces, Rep. Prog. Phys. **80**, 112001 (2017).

[19] Y. Zhang, C. Min, X. Dou, X. Wang, H. P. Urbach, M. G. Somekh, and X. Yuan, Plasmonic tweezers: for nanoscale optical trapping and beyond, Light Sci. Appl. **10**, 59 (2021).

[20] Y. Yang, Y. Ren, M. Chen, Y. Arita, and C. Rosales-Guzmán, Optical trapping with structured light: A review, Adv. Opt. Photonics **3**, 034001 (2021).

[21] G. Volpe *et al.*, Roadmap for optical tweezers, J. Phys. Photonics **5**, 022501 (2023).

[22] D. E. Chang, J. D. Thompson, H. Park, V. Vuletic, A. S. Zibrov, P. Zoller, and M. D. Lukin, Trapping and manipulation of isolated atoms using nanoscale plasmonic structures, Phys. Rev. Lett. **103**, 123004 (2009).

[23] A. Reiserer, C. Nölleke, S. Ritter, and G. Rempe, Ground-state cooling of a single atom at the center of an optical cavity, Phys. Rev. Lett. **110**, 223003 (2013).

[24] J. Lu, H. Yang, L. Zhou, Y. Yang, S. Luo, Q. Li, and M. Qiu, Light-induced pulling and pushing by the the synergic effect of optical force and photophoretic force, Phys. Rev. Lett. **118**, 043601 (2017).

[25] E. Lee, D. Huang, and T. Luo, Ballistic supercavitating nanoparticles driven by single Gaussian beam optical pushing and pulling forces, Nat. Commun. **11**, 2404 (2020).

[26] A. Novitsky, C.-W. Qiu, and H. Wang, Single gradientless light beam drags particles as tractor beams, Phys. Rev. Lett. **107**, 203601 (2011).

[27] J. Chen, J. Ng, Z. Lin, and C. T. Chan, Optical pulling force, Nat. Photonics **5**, 531 (2011).

[28] V. Kajorndejnukul, W. Ding, S. Sukhov, C.-W. Qiu, and A. Dogariu, Linear momentum increase and negative optical forces at dielectric interface, Nat. Photonics **7**, 787 (2013).

[29] V. Shvedov, A. R. Dovoyan, C. Hnatovsky, N. Engheta, and W. Krolikowski, A long-range polarization-controlled optical tractor beam, Nat. Photonics **8**, 846 (2014).

[30] H. Li, Y. Cao, L.-M. Zhou, X. Xu, T. Zhu, Y. Shi, C.-W. Qiu, and W. Ding, Optical pulling forces and their applications, Adv. Opt. Photonics **12**, 288 (2020).

[31] H. Li *et al.*, Momentum-topology-induced optical pulling force, Phys. Rev. Lett. **124**, 143901 (2020).

[32] L. Paterson, M. P. MacDonald, J. Arlt, W. Sibbett, P. E. Bryant, and K. Dholakia, Controlled rotation of optically trapped microscopic particles, Science **292**, 912 (2001).

[33] A. B. Stilgoe, T. A. Nieminen, and H. Rubinsztein-Dunlop, Controlled transfer of transverse orbital angular momentum to optically trapped birefringent microparticles, Nat. Photonics **16**, 346 (2022).

[34] O. Brzobohaty, V. Karasek, M. Siler, L. Chvatal, T. Cizmar, and P. Zemanek, Experimental demonstration of optical transport, sorting and self-arrangement using a "tractor beam," Nat. Photonics **7**, 123 (2013).

[35] P. Zemánek, G. Volpe, A. Jonáš, and O. Brzobohatý, Perspective on light-induced transport of particles: from optical forces to phoretic motion, Adv. Opt. Photonics **11**, 577 (2021).

[36] C. F. Bohren and D. R. Huffman, *Absorption and Scattering of Light by Small Particles* (John Wiley & Sons, New York, 2008).

[37] Y. Tang and A. E. Cohen, Optical chirality and its interaction with matter, Phys. Rev. Lett. **104**, 163901 (2010).

[38] K. Y. Bliokh and F. Nori, Characterizing optical chirality, Phys. Rev. A **83**, 021803(R) (2011).

[39] J. Mun, M. Kim, Y. Yang, T. Badloe, J. Ni, Y. Chen, C. Qiu, and J. Rho, Electromagnetic chirality: From fundamentals to nontraditional chiroptical phenomena, Light Sci. Appl. **9**, 139 (2020).

[40] F. J. Rodríguez-Fortuño, N. Engheta, A. Martínez, and A. V. Zayats, Lateral forces on circularly polarizable particles near a surface, Nat. Commun. **6**, 8799 (2015).

[41] M. Antognozzi, C. R. Bermingham, R. L. Harniman, S. Simpson, J. Senior, R. Hayward, H. Hoerber, M. R. Dennis, A. Y. Bekshaev, K. Y. Bliokh, and F. Nori, Direct measurements of the extraordinary optical momentum and transverse spin-dependent force using a nano-cantilever, Nat. Phys. **12**, 731 (2016).

[42] H. Magallanes and E. Brasselet, Macroscopic direct observation of optical spin-dependent lateral forces and left-handed torques, Nat. Photonics **12**, 461 (2018).

[43] H. Chen, H. Zheng, W. Lu, S. Liu, J. Ng, and Z. Lin, Lateral optical force due to the breaking of electric-magnetic symmetry, Phys. Rev. Lett. **125**, 073901 (2020).

[44] T. Zhu, Y. Shi, W. Ding, D. P. Tsai, T. Cao, A. Q. Liu, M. Nieto-Vesperinas, J. J. Sáenz, P. C. Wu, and C.-W. Qiu, Extraordinary multipole modes and ultra-enhanced optical lateral force by chirality, Phys. Rev. Lett. **125**, 043901 (2020).

[45] Y. Shi, T. Zhu, J. Liu, D. P. Tsai, H. Zhang, S. Wang, C. T. Chan, P. C. Wu, A. V. Zayats, F. Nori, and A. Q. Liu, Stable optical lateral forces from inhomogeneities of the spin angular momentum, Sci. Adv. **8**, eabn2291 (2022).

[46] J. Lu, V. Ginis, C.-W. Qiu, and F. Capasso, Polarization-dependent forces and torques at resonance in a micro-fiber-microcavity system, Phys. Rev. Lett. **130**, 183601 (2023).

[47] X. Yu, Y. Li, B. Xu, X. Wang, L. Zhang, J. Chen, Z. Lin, and C. T. Chan, Anomalous lateral optical force as a manifestation of the optical transverse spin, Laser Photonics Rev. **17**, 2300212 (2023).

[48] K. Y. Bliokh, A. Y. Bekshaev, and F. Nori, Extraordinary momentum and spin in evanescent waves, Nat. Commun. **5**, 3300 (2014).

[49] A. Y. Bekshaev, K. Y. Bliokh, and F. Nori, Transverse spin and momentum in two-wave interference, Phys. Rev. X **5**, 011039 (2015).

[50] A. Aiello, P. Banzer, M. Neugebauer, and G. Leuchs, From transverse angular momentum to photonic wheels, Nat. Photonics **9**, 789 (2015).

[51] J. S. Eismann, L. H. Nicholls, D. J. Roth, M. A. Alonso, P. Banzer, F. J. Rodríguez-Fortuño, A. V. Zayats, F. Nori, and K. Y. Bliokh, Transverse spinning of unpolarized light, Nat. Photonics **15**, 156 (2021).

[52] S. B. Wang and C. T. Chan, Lateral optical force on chiral particles near a surface, Nat. Commun. **5**, 3307 (2014).

[53] A. Hayat, J. P. Balthasar Mueller, and F. Capasso, Lateral chirality-sorting optical forces, Proc. Natl. Acad. Sci. U.S.A. **112**, 13190 (2015).

[54] T. Zhang, M. R. C. Mahdy, Y. Liu, J. H. Teng, C. T. Lim, Z. Wang, and C.-W. Qiu, All-optical chirality-sensitive sorting via reversible lateral forces in interference fields, ACS Nano **11**, 4292 (2017).

[55] B. Spivak and A. V. Andreev, Photoinduced separation of chiral isomers in a classical buffer gas, Phys. Rev. Lett. **102**, 063004 (2009).

[56] N. Kravets, A. Aleksanyan, and E. Brasselet, Chiral optical Stern-Gerlach Newtonian experiment, Phys. Rev. Lett. **122**, 024301 (2019).

[57] A. Canaguier-Durand, J. A. Hutchison, C. Genet, and T. W. Ebbesen, Mechanical separation of chiral dipoles by chiral light, New J. Phys. **15**, 123037 (2013).

[58] G. Tkachenko and E. Brasselet, Spin controlled optical radiation pressure, Phys. Rev. Lett. **111**, 033605 (2013).

[59] D. S. Bradshaw and D. L. Andrews, Chiral discrimination in optical trapping and manipulation, New J. Phys. **16**, 103021 (2014).

[60] G. Tkachenko and E. Brasselet, Optofluidic chiral sorting of material chirality by chiral light, Nat. Commun. **5**, 3577 (2014).

[61] M. Donato, J. Hernandez, A. Mazzulla, C. Provenzano, R. Saija, R. Sayed, S. Vasi, A. Magazzu, P. Pagliusi, R. Bartolino, P. Gucciardi, O. Marago, and G. Cipparrone, Polarization-dependent optomechanics mediated by chiral microresonators, Nat. Commun. **5**, 3656 (2014).

[62] G. Tkachenko and E. Brasselet, Helicity-dependent three-dimensional optical trapping of chiral microparticles, Nat. Commun. **5**, 4491 (2014).

[63] P. Acebal, L. Carretero, and S. Blaya, Design of an optical conveyor for selective separation of a mixture of enantiomers, Opt. Express **25**, 32290 (2017).

[64] T. Cao and Y. Qiu, Lateral sorting of chiral nanoparticles using fano-enhanced chiral force in visible region, Nanoscale **10**, 566 (2018).

[65] M. Li, S. Yan, Y. Zhang, Y. Liang, P. Zhang, and B. Yao, Optical sorting of small chiral particles by tightly focused vector beams, Phys. Rev. A **99**, 033825 (2019).

[66] Y. Shi, T. Zhu, T. Zhang, A. Mazzulla, D. P. Tsai, W. Ding, A. Q. Liu, G. Cipparrone, J. J. Sáenz, and C. Qiu, Chirality-assisted lateral momentum transfer for bidirectional enantioselective separation, Light Sci. Appl. **9**, 62 (2020).

[67] M. Li, X. Chen, S. Yan, Y. Zhang, and B. Yao, Enatioselective rotation of chiral particles by azimuthally polarized beams, Adv. Photonics Res. **3**, 2200117 (2022).

[68] L. Fang and J. Wang, Optical trapping separation of chiral nanoparticles by subwavelength slot waveguides, Phys. Rev. Lett. **127**, 233902 (2021).

[69] P. C. Chaumet and A. Rahmani, Electromagnetic force and torque on magnetic and negative-index scatterers, Opt. Express **17**, 2224 (2009).

[70] M. Nieto-Vesperinas, J. Sáenz, R. Gómez-Medina, and L. Chantada, Optical forces on small magnetodielectric particles, Opt. Express **18**, 11428 (2010).

[71] See Supplemental Material, which includes Refs. [27,36,52–54,68–70,72,73], at http://link.aps.org/supplemental/10.1103/PhysRevLett.133.233803 for optical forces exerted on chiral particles, optical chiral density distributions in the 3D focused fields of the full standard Poincaré sphere beams, expressions for the electromagnetic field vectors in the image space of an aplanatic system, and the control of trap positions and separation distances by means of desired input polarization parameters.

[72] B. Richards and E. Wolf, Electromagnetic diffraction in optical systems, II. Structure of the image field in an aplanatic system, Proc. R. Soc. A **253**, 358 (1959).

[73] M. Born and E. Wolf, *Principles of Optics*, 7th ed. (Cambridge University Press, Cambridge, England, 1999).

[74] K. S. Youngworth and T. G. Brown, Focusing of high numerical aperture cylindrical vector beams, Opt. Express **7**, 77 (2000).

[75] Q. Zhan, Cylindrical vector beams: From mathematical concepts to applications, Adv. Opt. Photonics **1**, 1 (2009).

[76] G. Milione, H. I. Sztul, D. A. Nolan, and R. R. Alfano, Higher-order poincaré sphere, stokes parameters, and the angular momentum of light, Phys. Rev. Lett. **107**, 053601 (2011).

[77] J. P. Balthasar Mueller, N. A. Rubin, R. C. Devlin, B. Groever, and F. Capasso, Metasurface polarization optics: Independent phase control of arbitrary orthogonal states of polarization, Phys. Rev. Lett. **118**, 113901 (2017).

[78] Y. Zhao, J. S. Edgar, G. D. M. Jeffries, D. McGloin, and D. T. Chiu, Spin-to-orbital angular momentum conversion in a strongly focused optical beam, Phys. Rev. Lett. **99**, 073901 (2007).

[79] Z. Man, Z. Xi, X. Yuan, R. E. Burge, and H. P. Urbach, Dual coaxial longitudinal polarization vortex structures, Phys. Rev. Lett. **124**, 103901 (2020).

[80] T. Cao, L. Mao, Y. Qiu, L. Lu, A. Banas, K. Banas, R. E. Simpson, and H. C. Chui, Fano resonance in asymmetric plasmonic nanostructure: Separation of sub-10 nm enantiomers, Adv. Opt. Mater. **7**, 1801172 (2018).